Sumie S, Nakashima O, Okuda K, Kuromatsu R, Kawaguchi A, Nakano M, Satani M, Yamada S, Okamura S, Hori M, Kakuma T, Torimura T, Sata M.	The Significance of Classifying Microvascular Invasion in Patients with Hepatocellular Carcinoma.	Ann Surg Oncol	Nov 20		2013
Kondo R, Nakashima O, Sata M, Imazeki F, Yokosuka O, Tanikawa K, Kage M, Yano H; The Liver Cancer Study Group of Kyushu.	Pathological characteristics of patients who develop hepatocellular carcinoma with negative results of both serous hepatitis B surface antigen and hepatitis C virus antibody.	Hepatol Res	Aug 13.		2013
Kondo R, Yano H, Nakashima O, Tanikawa K, Nomura Y, Kage M.	Accumulation of platelets in the liver may be an important contributory factor to thrombocytopenia and liver fibrosis in chronic hepatitis C.	J Gastroenterol.	Apr;48(4)	526-34.	2013
Utsunomiya T, Shimada M, Kudo M, Ichida T, Matsui O, Izumi N, Matsuyama Y, Sakamoto M, Nakashima O, Ku Y, Kokudo N, Makuuchi M; Liver Cancer Study Group of Japan.	Nationwide study of 4741 patients with non-B non-C hepatocellular carcinoma with special reference to the therapeutic impact.	Ann Surg	259 (2)	336-45	2014
Shindoh J, Hasegawa K, Matsuyama Y, Inoue Y, Ishizawa T, Aoki T, Sakamoto Y, Sugawara Y, Makuuchi M, Kokudo N.	Low hepatitis C viral load predicts better long-term outcomes in patients undergoing resection of hepatocellular carcinoma irrespective of serologic eradication of hepatitis C virus.	J Clin Oncol	31(6)	766-773	2013
Mise Y, Sakamoto Y, Ishizawa T, Kaneko J, Aoki T, Hasegawa K, Sugawara Y, Kokudo N.	A worldwide surgery of the current daily practice in liver surgery.	Liver Cancer	2(1)	55-66	2013
Tanaka Y, Nakazawa T, Komori S, Hidaka H, Okuwaki Y, Takada J, Watanabe M, Shibuya A, Minamino T, Yamamoto H, Kokubu S, Hayakawa K, Koizumi W.	Radiotherapy for patients with unresectable advanced hepatocellular carcinoma with invasion to intrahepatic large vessels: efficacy and outcomes.	Gastroenterol Hepatol			2013 [Epub ahead of print]

Nakazawa T, Hidaka H, Takada J, Okuwaki Y, Tanaka Y, Watanabe M, Shibuya A, Minamino T, Kokubu S, Koizumi W.	Early increase in α-fetoprotein for predicting unfavorable clinical outcomes in patients with advanced hepatocellular carcinoma treated with sorafenib.	Eur J Gastroenterol Hepatol	25(6)	683-9	2013
Hidaka H, Wang G, Nakazawa T, et al.	Total and viable residual splenic volume measurement after partial splenic embolization by three-dimensional ultrasound.	J Med Ultrasonics			2013 (in press)
Hidaka, H., Ohbu, M., Matsumoto, Y., Minamino, T., Takada, J., Tanaka, Y., Okuwaki, Y., Watanabe, M., Nakazawa, T., Shibuya, A. and Koizumi, W.	Olmesartan for non-alcoholic steatohepatitis complicated with hypertension: An open-label study.	Open Journal of Gastroenterology	3	128-133	2013
Hidaka H, Nakazawa T, Kutsukake S, Yamazaki Y, Aoki I, Nakano S, Asaba N, Minamino T, Takada J, Tanaka Y, Okuwaki Y, Watanabe M, Shibuya A, and Koizumi W.	The efficacy of nocturnal administration of branched-chain amino acid granules to improve quality of life in patients with cirrhosis.	J Gastroenterol	48	269-276	2013
Arao T, Ueshima K, Matsumoto K, Nagai T, Kimura H, Hagiwara S, Sakurai T, Haji S, Kanazawa A, Hidaka H, Iso Y, Kubota K, Shimada M, Utsunomiya T, Hirooka M, Hiasa Y, Toyoki Y, Hakamada K, Yasui K, Kumada T, Toyoda H, Sato S, Hisai H, Kuzuya T, Tsuchiya K, Izumi N, Arii S, Nishio K, Kudo M.	FGF3/FGF4 amplification and multiple lung metastases in responders to sorafenib in hepatocellular carcinoma.	Hepatology	57(4)	1407-15	2013

Ⅳ. 研究成果の刊行物・別刷

Oncology

Oncology 2013;84(suppl 1):3–12
DOI: 10.1159/000345883

Published online: February 20, 2013

Novel Image Analysis Method Using Ultrasound Elastography for Noninvasive Evaluation of Hepatic Fibrosis in Patients with Chronic Hepatitis C

Kenji Fujimoto[a, b] Michio Kato[b] Masatoshi Kudo[c] Norihisa Yada[c] Tsuyoshi Shiina[d] Kazuomi Ueshima[c] Yukinori Yamada[e] Tetsushi Ishida[f] Masayoshi Azuma[f] Masaru Yamasaki[g] Keiji Yamamoto[b] Norio Hayashi[h] Tetsuo Takehara[i]

[a]Division of Clinical Research and [b]Department of Internal Medicine, National Hospital Organization Minamiwakayama Medical Center, Tanabe, [c]Department of Gastroenterology and Hepatology, Kinki University School of Medicine, Osakasayama, [d]Human Health Sciences, Graduate School of Medicine, Kyoto University, Kyoto, Departments of [e]Gastroenterology and Hepatology, [f]Internal Medicine and [g]Clinical Laboratory, Kaizuka City Hospital, Kaizuka, [h]Department of Gastroenterology and Hepatology, Japan Labour Health and Welfare Organization, Kansai Rousai Hospital, Amagasaki, and [i]Department of Gastroenterology and Hepatology, Osaka University Graduate School of Medicine, Suita, Japan

Key Words
Real-time tissue elastography · Chronic hepatitis · Ultrasound elastography · Liver fibrosis

Abstract
It has been established that the long-term infection of chronic hepatitis C leads to the increased risk of hepatic fibrosis and hepatocellular carcinoma. Currently, histological diagnosis by invasive and painful liver biopsy is the gold standard for evaluating the hepatic fibrosis stage. Because of a side effect or patient inability to cope with the pain, it is difficult to assess the fibrosis stage frequently using liver biopsy. Recently, instead of liver biopsy, many articles have been published showing the usefulness of ultrasound elastography to evaluate the stage of hepatic fibrosis. We also reported the usefulness of real-time tissue elastography (RTE) for liver fibrosis staging in 2007. However, in our previous report, fibrosis classification was performed manually and the number of patients involved was also small. In the current study, the fibrosis staging is performed automatically using software by characterizing the elastography images. We have also increased the number of patients from 64 to 310. Thus, the aim of this study is to increase objectivity by using a newly developed automatic analysis method. We obtain the Liver Fibrosis Index (LFI), which is calculated from image features of RTE images, using multiple regression analysis performed on clinical data of 310 cases as the training data set. The correlation coefficient obtained between the LFI and the stage of hepatic fibrosis was $r = 0.68$, and significant differences exist between all stages of fibrosis ($p < 0.001$). Our new method seems promising since it has the ability to diagnose fibrosis even in the presence of inflammation.

Introduction

Approximately 700,000 people worldwide are estimated to die annually of hepatocellular carcinoma (HCC), which is the third highest cause of cancer death [1, 2]. HCC often develops in the presence of hepatic fibrosis from long-term infection of chronic hepatitis B and C. It has been reported that the risk of HCC increases as the stage of liver fibrosis progresses [3]. It has been shown that fibrosis treatment using interferon reduces hepatic

KARGER
Fax +41 61 306 12 34
E-Mail karger@karger.com
www.karger.com

0030–2414/13/0847–0003$38.00/0

Accessible online at:
www.karger.com/ocl

Masatoshi Kudo, MD, PhD
Division of Gastroenterology and Hepatology, Department of Internal Medicine
Kinki University Faculty of Medicine
377-2 Ohno-Higashi, Osakasayama, Osaka 589-8511 (Japan)
E-Mail m-kudo@med.kindai.ac.jp

Abbreviations used in this paper

MEAN	Mean of relative strain value within the ROI
SD	Standard deviation of relative strain value within the ROI
%AREA	Area of low strain (blue) within the ROI
COMP	Complexity of low strain (blue) area within the ROI = (perimeter)^2/area
SKEW	Skewness – asymmetry of the histogram
KURT	Kurtosis – peakedness of the histogram
ENT	Entropy – textural complexity
IDM	Inverse Difference Moment – textual local homogeneity
ASM	Angular Second Moment – textual homogeneity

fibrosis and also dramatically reduces the incidence of HCC [4]. Thus, it is important to evaluate the stage of hepatic fibrosis both for establishing treatment and also for monitoring its effectiveness.

Histological diagnosis using liver biopsy is very important for the evaluation of hepatic fibrosis [5–10]. However, because of its invasiveness, liver biopsy cannot be performed frequently. In addition, there is a limitation in the accuracy of liver biopsy due to sampling error [11–13]. Thus, the development of noninvasive tests that are reliable, cost-effective and easy to use is required for evaluating the stage of hepatic fibrosis. Previously, measurement of platelet counts [14] and liver fibrosis marker [15–18] were used as noninvasive tests to evaluate hepatic fibrosis, but generally the basic procedure for evaluating the stage of hepatic fibrosis is to combine the use of these tests with diagnostic imaging techniques, such as ultrasonography.

Ultrasound imaging is the most useful imaging diagnostic technique used for evaluating chronic hepatitis and/or cirrhosis. The image characteristics for evaluating hepatic fibrosis/cirrhosis are the nodular liver parenchyma, heterogeneous internal echo texture, decrease in the volume of right hepatic lobe and increase in the volume of caudate and left hepatic lobe, and the narrowing of the hepatic vein [19, 20]. However, staging of the liver fibrosis using these characteristics is less reliable since the appearance of images can be changed due to differences in ultrasonic power and/or the image settings of the equipment used. Ultrasound tissue characterization has been attempted in the literature for objective evaluation of tissue by analyzing the signals obtained from the ultrasound system, for example intensity of RF signals, extent of scattering [21, 22] and velocity of shear wave generated by a probe in the liver [23].

New methods are emerging to estimate the liver stiffness or the fibrosis, using ultrasound elastography or MRI [24]. There are many forms of elastography that are popular, namely transient elastography (Fibroscan®) [25–28], acoustic radiation forces impulse imaging (ARFI) and our own real-time tissue elastography (RTE) [29–32]. Fibroscan and ARFI measure the velocity of shear waves propagating in the tissue to measure liver stiffness, which is then correlated to fibrosis. However, in the case of Fibroscan, measured liver stiffness is correlated not only with the stage of hepatic fibrosis, but also with grade of inflammation. Therefore, the involvement of many dynamic factors independent of hepatic fibrosis affect the measurement value, such as inflammation or cholestasis. The stage of hepatic fibrosis, which is the goal of the imaging technique, should be defined as the parameter dependent only on the fibrosis of the liver, which is the true pathology to be indicated and should not include other dynamic factors.

Our RTE is different from Fibroscan and ARFI and it measures relative stiffness of the tissue in the region of interest (ROI) and displays the stiffness with color overlaid over the B-mode image in real time. Apart from liver imaging, it has many other clinical applications that have been reported in the literature, such as breast, thyroid, prostate and pancreas [33–36]. RTE image is constructed using tissue strains which are calculated from 2 consecutive frames. The phase difference of RF signals from 2 consecutive frames are calculated to obtain tissue strain and transferred to color codes. The colors in the ROI range from blue to red to show the relative hardness and softness of area inside the ROI [30, 31]. The harder areas are displayed in blue and the softer areas in red.

In our previous work using RTE for liver imaging, we established the usefulness of RTE for the evaluation of hepatic fibrosis of chronic hepatitis C patients. The reported liver elasticity scores, which were scored visually, showed significant correlation with hepatic fibrosis [37]. Our RTE, available as a native mode in an ultrasound system, can be used for evaluating patients even with ascites and severe hepatic atrophy.

Even though our previous paper showed the feasibility of using RTE, the main limitation was that the evaluation of the RTE images was performed visually. While evaluating visually, two radiologists used the increase in a blue area in the RTE image as a criteria for staging hepatic fibrosis. Blue areas of RTE images increased and became patchy as the stage of hepatic fibrosis increased. It was difficult for the radiologists to visually estimate hepatic fibrosis with RTE images since the scoring of fibrosis also depended on the individual examiner's image perspective. In addition, in our previous report, we did not perform any investigation about the relationship between the grade of inflammation and the RTE image. Thus, the aims of this study are: (1) to present a newly developed

image analysis software method to obtain Liver Fibrosis Index (LFI) automatically from image features of RTE images using multiple regression analysis [38–40], (2) to show the effectiveness of this software tool and (3) to establish the relationship between LFI, the stage of fibrosis and the grade of inflammation.

Patients and Methods

Patients

The protocol was created following the Declaration of Helsinki and approved by an independent ethics committee of 3 institutions. For this study, we chose 295 patients with chronic hepatitis C or cirrhosis. Fifty-five patients were excluded from the study (table 1). All these patients were anti-hepatitis C virus and hepatitis C virus RNA positive, and were diagnosed by liver biopsy between May 2005 and December 2009. The patient population included 130 males and 165 females aged between 26 and 76 years old (mean age 56 years; table 1). Fifteen healthy volunteers were also enrolled as a normal control group. We obtained written informed consent from all participants at the National Hospital Organization Minamiwakayama Medical Center, Kaizuka City Hospital and Kinki University Hospital.

Liver Histology

Liver biopsy was performed twice using 18G automatic cutting biopsy needles (Adjustable Temno Biopsy System; Cardinal Health, Waukegan, Ill., USA) under local anesthesia for all study patients. Regardless of benign or malignant tumor, patients who had tumor located in the imaging plane from the right intercostal were excluded from the study. The specimen lengths were 20 mm (range 10–25 mm) and the sections were stained with hematoxylin and eosin and Masson trichrome staining. These sections were examined by 3 pathologists to stage the fibrosis and also to grade the activities. All 3 pathologists were blinded to any clinical data including the results of RTE. Hepatic fibrosis were staged from F0 to F4 according to the following scale: F0 – no fibrosis, F1 – portal fibrosis without septa, F2 – portal fibrosis with septa, F3 – numerous septa without cirrhosis and F4 – cirrhosis. Inflammatory activities were graded from A0 to A3 with the following scale: A0 – no activity, A1 – mild activity, A2 – moderate activity and A3 – severe activity.

The fifteen healthy volunteers were all male, aged between 22 and 52 years (average 31.5), BMI between 17.9 and 24.7 (average 21.0) and their blood tests, such as aspartate aminotransaminase, alanine transaminase, gamma-GTP, total cholesterol and triglyceride, were all within normal limits. All volunteers had no sign of fatty liver in ultrasonography findings, thus no liver biopsy was performed and they were staged F0.

Real-Time Tissue Elastography

HI VISION 900 (Hitachi Medical Corp., Tokyo, Japan) was used for ultrasonography and the probes used were EUP-L52 linear probes (7–3 MHz). We used linear array probes for this study over convex array probes because linear probes have many advantages when internal compression and relaxation induced by the cardiac motion is utilized for obtaining RTE images of the liver. We utilized internal compression and relaxation induced by the cardiac motion instead of manual compression because this is more consistent and reliable. Even though the field of view of a linear array probe is small, the direction of displacement induced by cardiac movement can be set to the surface of the probe, thus making it suitable for RTE analysis. Also, at smaller depth the field of view of a linear probe is much larger than that of convex probes, thus making it more suitable for an RTE image.

After obtaining B-mode images, the ultrasound mode was switched to RTE and scanned from the right intercostal space to observe the right hepatic lobe. RTE images were obtained by holding the probe still at the position where displacement by the cardiac motion in B-mode was in the axial direction. The optimum intercostal space was the position where liver parenchyma was imaged in the deepest area. When the liver was not contracted, RTE images were easily obtained by scanning through the intercostal space of anterior to middle axillary lines. Because the RTE image is formed from the strain values computed from the axial displacement, the position where liver parenchyma moves in a lateral direction due to cardiac motion was not suitable for this study.

The ROI for RTE was set inside liver parenchyma. Regions with large vessels or regions having shadows from ribs were avoided to reduce the artifacts arising from the anechoic region. The tops of the ROI were positioned at a depth of more than 1 cm from the surface of the liver to avoid multiple reflections arising from the surface of the liver.

RTE was performed using a freehand technique, with the linear probe placed at the appropriate position with the patient holding their breath. As mentioned in the previous paragraph, no manual compression/relaxation was applied. The compression/

Table 1. Background of patients and excluded cases

Patients (n = 295)	
Male/female	130/165
Age, years	56 ± 18
Range	26 – 76
ALT, IU/l	59.4 ± 41.1
Total bilirubin, mg/dl	0.9 ± 0.5
Albumin, g/dl	4.0 ± 1.1
Choline esterase, IU/l	270.4 ± 78.4
Total cholesterol, mg/dl	187.4 ± 33.4
Prothrombin time, %	94.2 ± 12.9
Platelet count ($\times 10^4/\mu l$)	16.2 ± 7.7
Fibrosis stage, F0/F1/F2/F3/F4	84/97/65/48
Histological activity, A0/A1/A2/A3	29/90/146/30
Excluded cases (n = 55)	
Poor penetration (n = 20)	
Fatty layer ≥5 mm and muscular layer ≥10 mm	9
Fatty layer ≥5 mm and muscular layer <10 mm	3
Fatty layer <5 mm and muscular layer ≥10 mm	5
Fatty layer <5 mm and muscular layer <10 mm	3
Unstable technique (n = 35)	
Slipping section by body movement	10
Slipping horizontally by cardiac movement	13
Poor cardiac movement	3
Artifact by multiple reflection	9

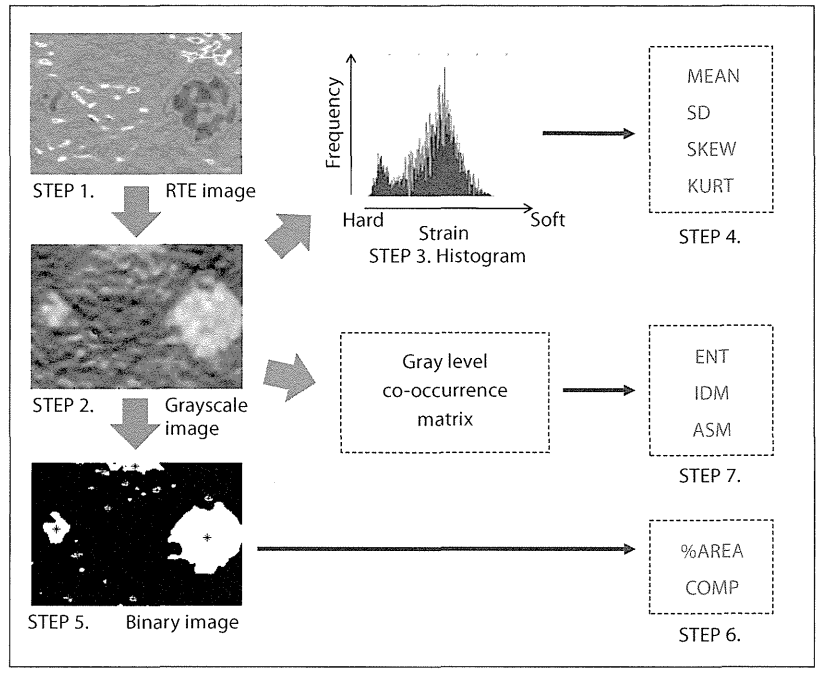

Fig. 1. Flow of calculations.

relaxation of the liver induced by the cardiac motion is easily detected to compute strain images. The ultrasound system parameters such as depth, ROI and gain were set for optimum RTE image quality. RTE images obtained by the lateral movements of the heart were avoided. One to two RTE images are displayed in 1 heartbeat, and the best RTE image was selected for final analysis. In total 3–5 RTE images obtained from different heart cycles without lateral motion were selected. The average of these 3–5 images for each patient was then used in regression analysis.

We extracted the following 9 image features to quantify the patchy pattern of the RTE images. More details about these features can also be found in the literature [41].

All 9 parameters have been found in the literature to be very useful for characterizing the imaging pattern in many different applications, e.g. satellite imaging, geothermal imaging and machine visions [42]. For liver fibrosis staging using RTE images, we employ these features for characterizing the image and correlating them with fibrosis staging. Analysis of RTE image features were performed with the prototype analysis software shown in figure 1. This software converts the selected analysis area of the RTE image (STEP 1) into a 256-step grayscale image (STEP 2), plots the strain histogram (STEP 3), and calculates the mean of relative strain (MEAN), standard deviation of relative strain (SD), skewness of strain histogram (SKEW) and kurtosis of strain histogram (KURT; STEP 4). Moreover, it binarizes the RTE image into black and white regions: white as low strain (blue) regions and black as all other regions (STEP 5). To characterize the low strain (blue) regions of the binary image, it calculates the ratio of low strain regions within the selected analysis area (%AREA), and the complexity of the low strain region (COMP; STEP 6). Furthermore, it also calculates entropy (ENT), inverse difference moment (IDM), and angular second moment (ASM) to evaluate the texture of the RTE image (STEP 7). Multiple regression analysis was then performed to improve the diagnostic accuracy using all these 9 image features instead of diagnosing with individual image features.

The LFI was estimated using these 9 image features as independent variables and the hepatic fibrosis stage as a dependent variable, as shown in the following multiple regression equation:

$$\begin{aligned}\text{LFI} = {} & -0.009 \times \text{MEAN} - 0.005 \times \text{SD} + 0.023 \times \%\text{AREA} \\ & + 0.025 \times \text{COMP} + 0.775 \times \text{SKEW} - 0.281 \times \text{KURT} \\ & + 2.083 \times \text{ENT} + 3.042 \times \text{IDM} + 39.979 \times \text{ASM} - 5.542.\end{aligned}$$

Multiple regression analysis was also performed to estimate the Liver Activity Index (LAI) using 9 image features as independent variables and grade of inflammatory activity as a dependent variable. LFI and LAI were calculated for all patients and compared with the stage of hepatic fibrosis and grade of inflammatory activity. Then, to eliminate the inflammatory activity from hepatic fibrosis, LAI and grade of inflammatory activity were compared for each stage of hepatic fibrosis. Receiver operating characteristic (ROC) analysis was performed for LFI to obtain a cutoff value for the identification of F0–1/F2–4 and F0–3/F4, and also to calculate sensitivity, specificity, accuracy and area under ROC (AUROC).

Statistical Analysis

All of the statistical analysis, such as multiple regression analysis and ROC analysis were carried out using the JMP statistical discovery software, version 8.0 (SAS Institute Inc., Cary, N.C., USA) for windows.

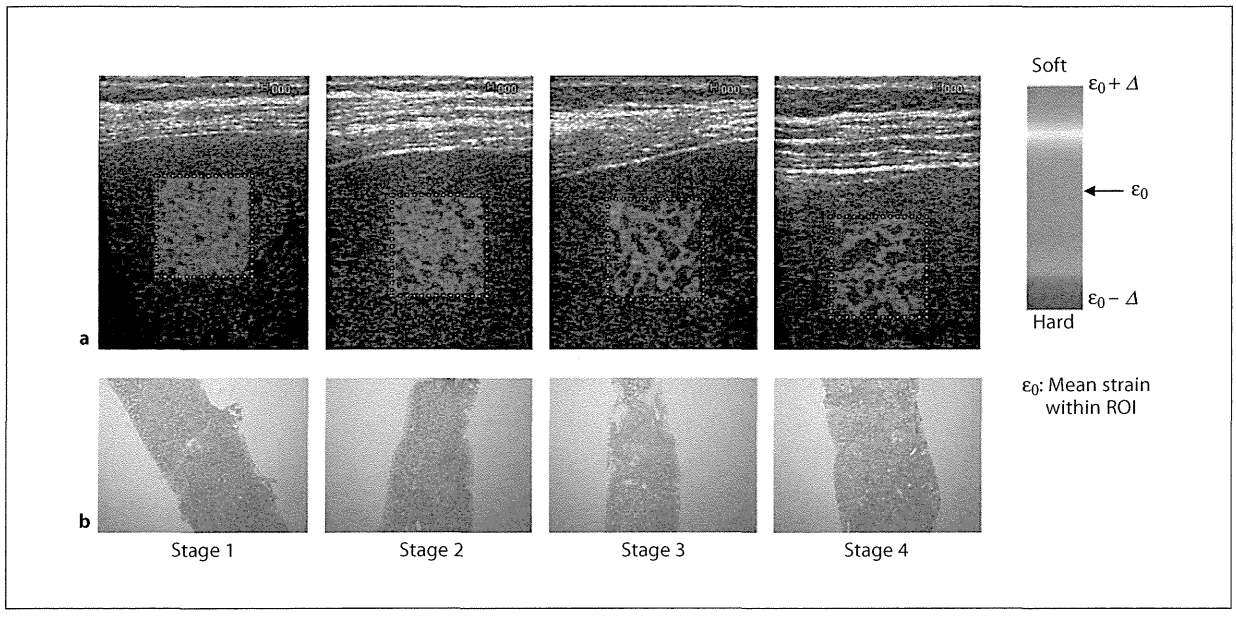

Fig. 2. RTE images (**a**) and pathological images, Masson trichrome stain, ×100 (**b**).

Results

Patients

We performed liver elastography in 365 patients (including 15 healthy volunteers) between April 2005 and November 2009. We excluded 55 patients from our study because more than 3 stable RTE images could not be acquired for these patients. Most of the reasons of exclusion were related to RTE skill of the clinicians, which improved significantly with more experience. Table 1 shows the characteristics of the 295 patients (excluding 15 healthy volunteers out of 310 patients). The indicated stages of hepatic fibrosis in the study patients were: F0 in 1 subject, F1 in 84 subjects, F2 in 97 subjects, F3 in 65 subjects and F4 in 48 subjects. The stage of hepatic fibrosis in all healthy volunteers was F0. Typical RTE images and pathological images for each fibrosis stage are shown in figure 2.

Correlation between Features and Stage

In the present study, as described previously, we extracted 9 image features. Correlation coefficients between 9 image features, such as MEAN, SD, %AREA, COMP, SKEW, KURT, ENT, IDM and ASM and stage of hepatic fibrosis were −0.63, 0.53, 0.65, 0.58, 0.59, 0.02, −0.22, 0.34 and 0.21, respectively. Thus, 5 of 9 image features, i.e. MEAN, SD, %AREA, COMP and SKEW, highly correlated with the stage of hepatic fibrosis (fig. 3).

Accuracy of Staging Fibrosis by LFI

Figure 4 shows the relationship between hepatic fibrosis stages and LFI calculated from 9 image features using multiple regression analysis. LFI highly correlates with the fibrosis stages ($r = 0.68$ with $p < 0.001$), and significant differences exist between all different stages. Figure 5 shows the ROC analysis. When the cutoff value of LFI was set to 1.92, the AUROC of LFI for F0–1 versus F2–4 was 0.82, and sensitivity, specificity and accuracy were 78.6, 78.0 and 78.4%, respectively. For F0–3 versus F4, when the cutoff value was 2.56, the AUROC was 0.87, and sensitivity, specificity and accuracy were 79.2, 80.5 and 80.3%, respectively (fig. 5). In this study, LFI clearly differentiates either F0–1 and F2–4 or F0–3 and F4.

Effect of Inflammation

Figure 6 shows the comparison between grades and the 9 image features for evaluating the effect of inflammation on RTE image. None of the 9 image features have a correlation with grades, and LAI, which was calculated by multiple regression analysis similar to LFI, also did not correlate with grades ($r = 0.30$; fig. 6j).

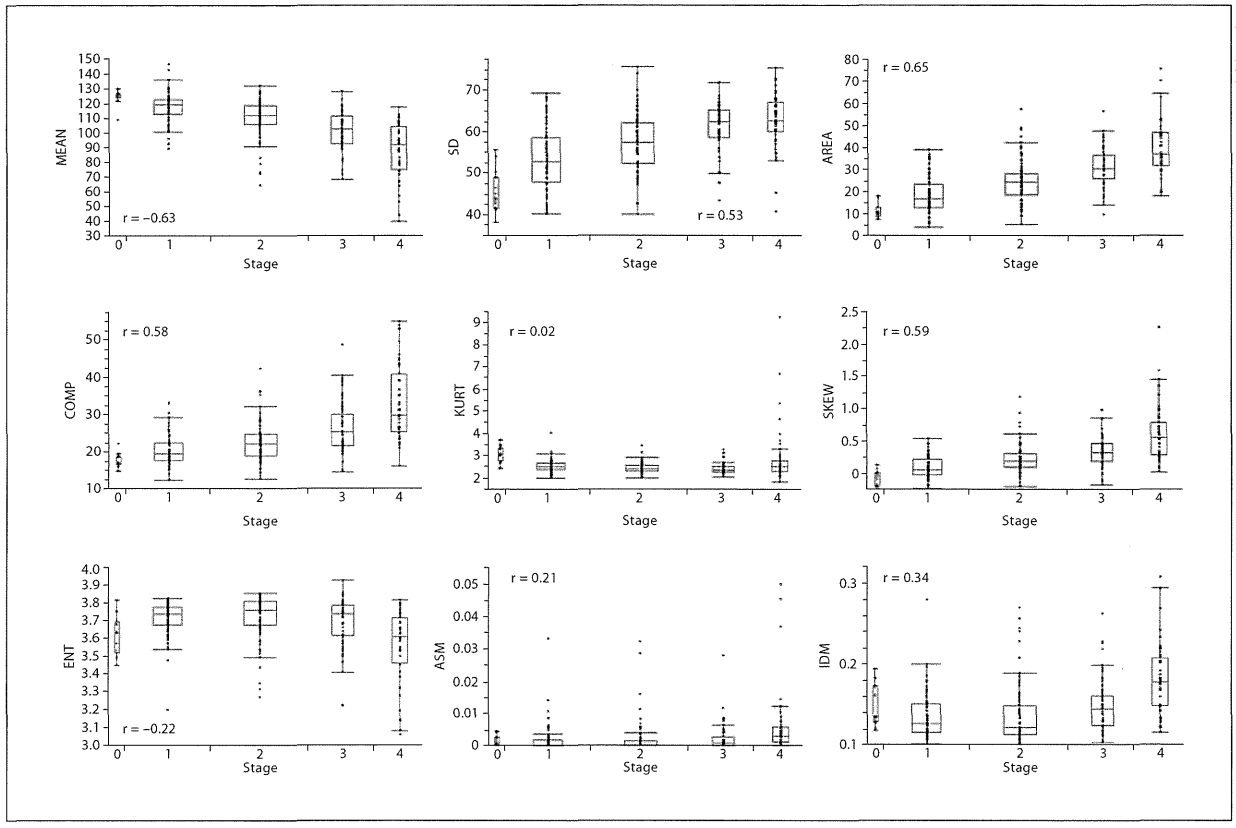

Fig. 3. Comparisons of stage of hepatic fibrosis and image features.

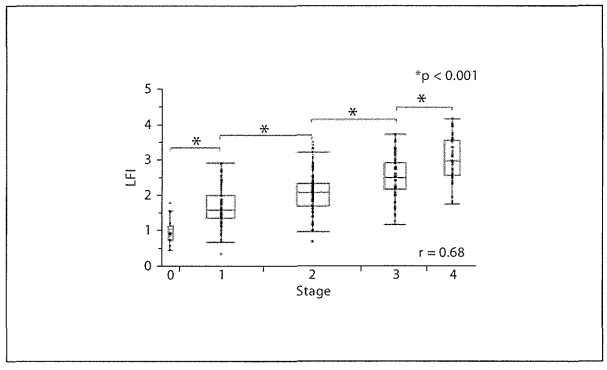

Fig. 4. Comparison of stage of hepatic fibrosis and LFI.

Discussion

Results of Estimation

To improve the accuracy of estimation of hepatic fibrosis and to make it automatic, we performed multiple regression analysis using 9 image features and obtained the estimated LFI. This index highly correlated with the stage of hepatic fibrosis ($r = 0.68$, $p < 0.001$) and significant differences were also observed between each stage. Furthermore, ROC analysis indicated that LFI has a high ability to differentiate each stage.

All 9 image features we used are independent and do not include confounding factors. Out of the 9 image features we analyzed, 5 (%AREA, MEAN, SD, COMP and SKEW) had a high correlation with the stages of hepatic fibrosis. This strong correlation, we believe, is mainly due to following reasons:

- AREA: hard area increases as a hepatic fibrosis progresses.

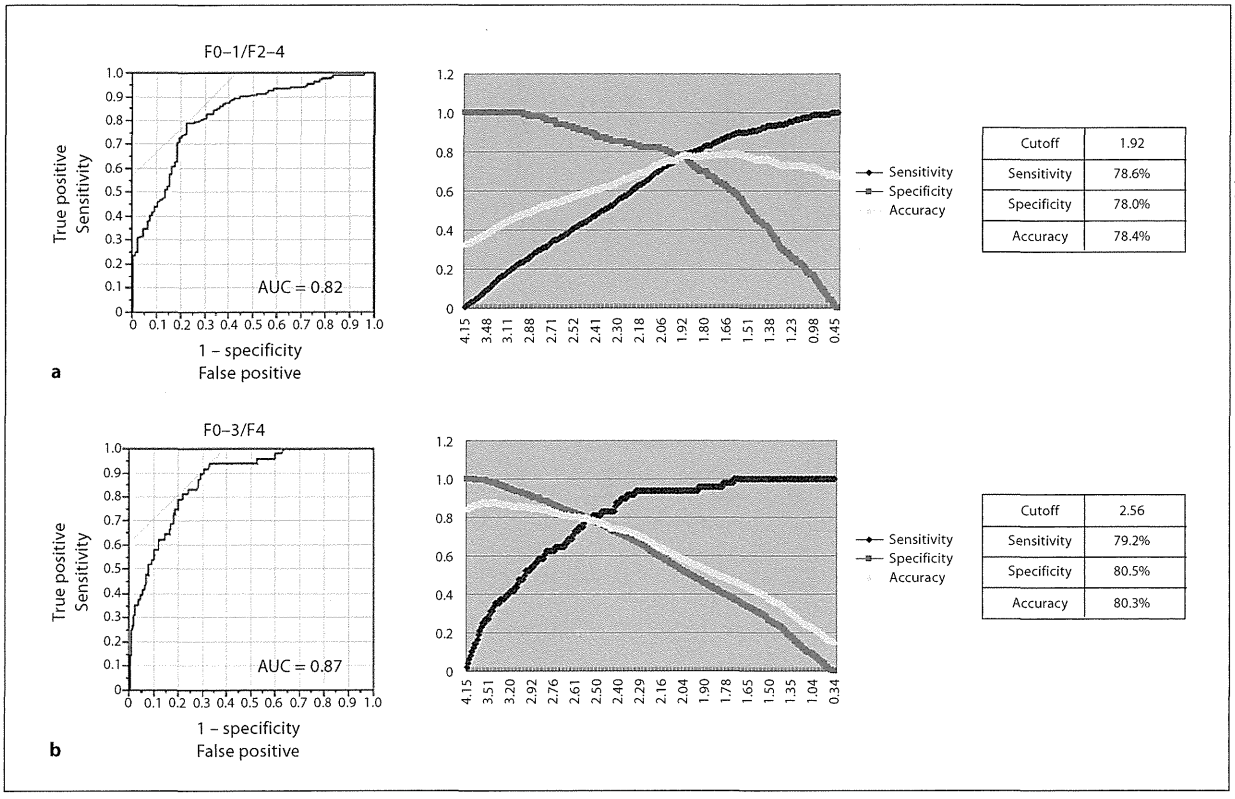

Fig. 5. ROC analysis differentiating F2–4 from F0–1 (**a**) and F4 from F0–3 (**b**).

- MEAN: liver parenchyma becomes stiffer as hepatic fibrosis progresses.
- SD: stiffness of liver parenchyma becomes heterogeneous as hepatic fibrosis progresses.
- COMP: figure of hard area becomes more complex as hepatic fibrosis progresses.
- SKEW: histogram skew towards the lower value of strain (harder) as hepatic fibrosis progresses.

Histopathological tissue evaluation using liver biopsy has been the gold standard for evaluation of hepatic fibrosis. However, this procedure is invasive, painful and could cause complications, such as hemorrhage, due to which many patients hesitate over the procedure. In addition, if the platelet count is low, partial thromboplastin time is greater than 3 s, the liver presents with a tumor and there is presence of ascites, then liver biopsy is also difficult to perform. This liver biopsy is also an economic burden due to the hospitalization required after the procedure. Currently, in such patients where a liver biopsy cannot be performed it is substituted with blood tests, which have significantly lower accuracy. Thus, our LFI based on RTE images, which is painless, cost-effective and can be performed in the presence of any of the above conditions can be a good addition to the clinicians tools for the noninvasive evaluation of liver fibrosis.

Effect of Inflammation

We did not find any correlation between any of the 9 features we used and inflammation grades. The RTE image, we believe, thus reflects the hepatic fibrosis and does not reflect the inflammatory factors such as intracellular pressure and change in blood flow due to inflammation. In addition, the spatial resolution of RTE images is 0.5–2 mm [43], which can completely capture the regenerating nodules in liver cirrhosis, which are 3–10 mm in size [44]. Thus, we can conclude that the LFI we have developed is not influenced by inflammation and it depends mainly upon liver fibrosis. Compared to RTE, other shear wave elastogra-

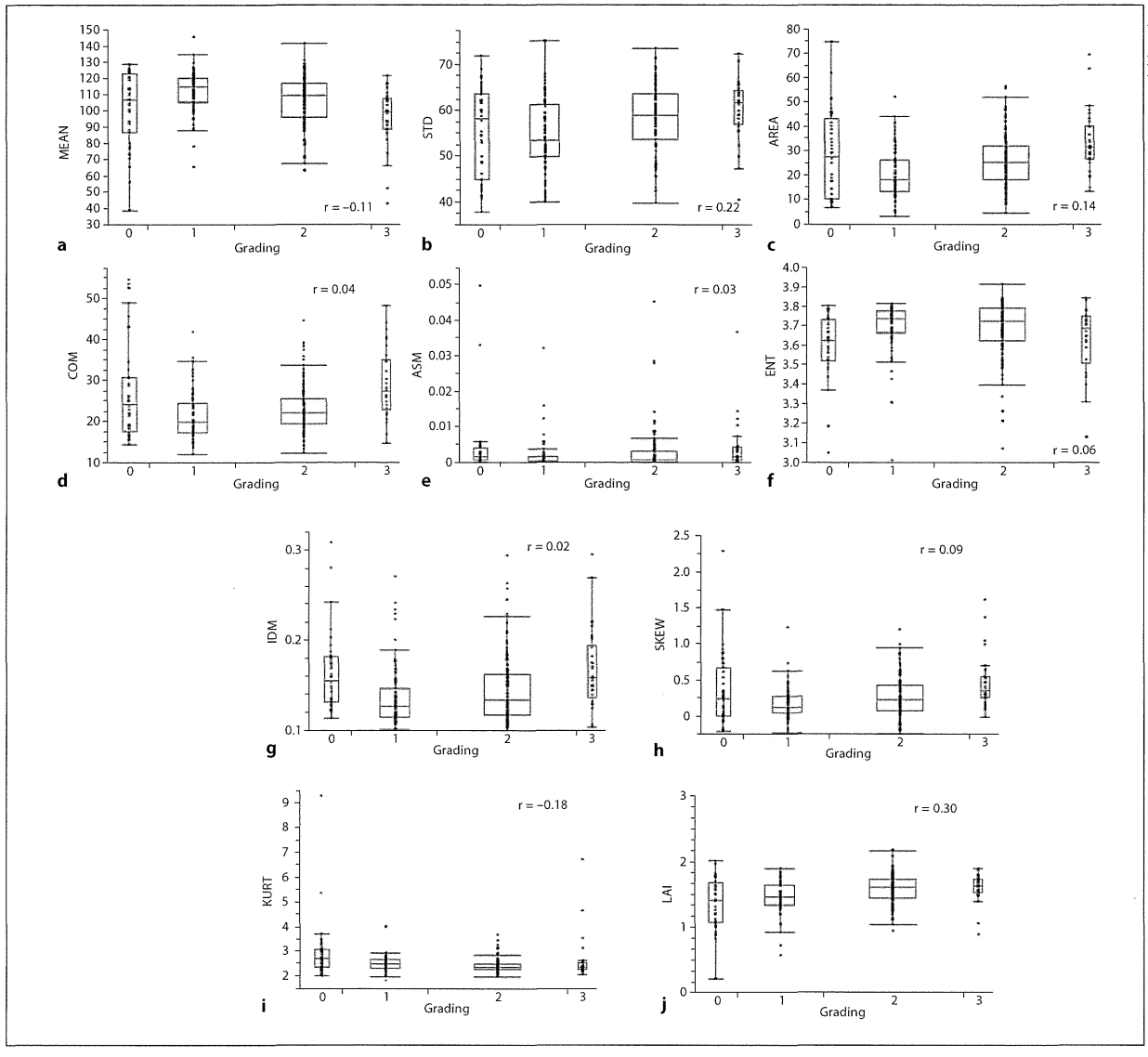

Color version available online

Fig. 6. a–j Comparison of grade and image features.

phy-based techniques, such as Fibroscan and ARFI, have been reported showing strong correlation with inflammation [45–47]. This correlation could be mainly because shear wave elastography adopts the principle of measuring the velocity of shear wave. Inflammatory factors such as intracellular pressure and condition of blood flow may change the velocity of shear waves, thus resulting in bias in the estimate.

Acquisition of RTE

We utilized compression/relaxation induced by the cardiac motion to obtain our RTE images for liver index computation. This helped to simplify RTE image acquisition and made it easier for clinicians to acquire RTE images. However, for some patients with weak pulsation and/or who are obese, it was difficult to perform liver elastography accurately. Training of clinicians was needed to avoid artifacts related to obesity, to set the ROI not

to include vessels and to adjust the position of the probe to image the liver where compression/relaxation was homogeneous and axial to the probe. RTE data were collected in 3 hospitals and 2 experts performed liver elastography. Image features were extracted from multiple RTE images and the average value from the acquired RTE images were used for our analysis.

Patient Selection Bias

In our study we did not include patients who had difficulty holding their breath or for whom it was difficult to image the liver through the intercostal spaces due to overlying bowel gases. Moreover, we excluded 55 cases with difficulty in analysis, the reasons for which are shown in table 1. The acquisition rate was 84.9% (310/365), which is still quite impressive in spite of these exclusions. Most of the exclusions happened at the beginning of the study. As the clinician gained experience, the failure rate reduced significantly and the success rate increased up to 98.0% (98/100). This implies that with some education and training the acquisition failure rate can be decreased significantly.

Limitations

We compared the results of LFI derived from RTE images with histopathological results of liver biopsy. However, liver biopsy results themselves have bias due to sampling error and due to the histopathological image being classified not by continuous quantity but staged by the progression of hepatic fibrosis. Moreover, there are large differences in the progression of hepatic fibrosis between 4 stages of liver fibrosis [40], thus the accuracy of liver biopsy is limited. Since liver biopsy results are used as a training set for our LFI computation, we speculate that there is also some bias in our estimate of liver fibrosis. A new index is needed as training data to derive a multiple regression equation to reduce the variation in results.

As a future subject for increasing the accuracy of the LFI, fibrosis staging by two or more pathologists is due to be judged using the block specimen by a surgical resection. Thereby, since the variation in a pathology result can be decreased, we think that better equation estimates of LFI can be derived.

Prospects of RTE

Our results of liver fibrosis staging are very impressive. It is automatic, consistent and agrees very well with current liver biopsy results. Thus, in the near future, we expect that the RTE could be used as a first-choice imaging tool for fibrosis screening. If considered suspicious, then liver biopsy can be performed for further confirmation. In addition, RTE imaging could be the only choice available along with blood tests for patients in whom liver biopsy cannot be performed. RTE can also be used for monitoring the progress or resolution of fibrosis in patients treated with interferon. It can also be used to monitor the progress in fibrosis in patients where interferon treatment was not done. RTE imaging is easy to use, cost-effective and, moreover, painless. It is readily available with the ultrasound machine as an additional mode making the technique easily available and easy to use when liver screening is being done to monitor cirrhosis and rule out HCC. It can also be used in patients with hepatitis other than viral, such as nonalcoholic steatohepatitis, etc.

Conclusion

LFI computed from RTE images highly correlates with stages of hepatic fibrosis and accurately reflects the underlying hepatic fibrosis, even with the presence of inflammation. Thus, it can be used for screening, monitoring and at times diagnosis of hepatic fibrosis. We believe our results and our techniques are superior to other techniques such as transient elastography. In the near future we plan to conduct more extensive clinical studies both for substantiating our results as well as to prove the clinical utility of RTE imaging for liver fibrosis staging.

Acknowledgments

We would like to thank Akiko Tonomura, Tsuyoshi Mitake, Mitsuru Motoki, Tomoko Furuta, MD, Chie Tatsumi, MD, Shigeo Wada, MD and Masahide Oshita, MD, for valuable contributions to this study.

Disclosure Statement

The authors declare that no conflicts of interest exist.

References

1 WHO International Agency for Research on Cancer: World Cancer Report 2008. Section 1 – global cancer control, chapter 1.3: worldwide cancer burden. http://www.iarc.fr/en/publications/pdfs-online/wcr/2008/index.php.

2 WHO International Agency for Research on Cancer: World Cancer Report 2008. Section 2 – etiology of cancer, chapter 2.5: chronic Infections.

3 Yoshida H, Shiratori Y, Moriyama M, et al: Interferon therapy reduces the risk for hepatocellular carcinoma: national surveillance program of cirrhotic and noncirrhotic patients with chronic hepatitis C in Japan. Ann Intern Med 1999;131:174–181.
4 Shiratori Y, Imazeki F, Moriyama M, et al: Histologic improvement of fibrosis in patients with hepatitis C who have sustained response to interferon therapy. Ann Intern Med 2000;132:517–524.
5 Desmet VJ, Gerber M, Hoofnagle JH, et al: Classification of chronic hepatitis: diagnosis, grading and staging. Hepatology 1994; 19:1513–1520.
6 Ichida F, Tsuji T, Omata M, et al: Classification report: new inuyama classification for histological assessment of chronic hepatitis. Internat Hepatol Comm 1996;6:112–119.
7 Ishak K, Baptista A, Bianchi L, et al: Histological grading and staging of chronic hepatitis. J Hepatol 1995;22:696.
8 Bataller R, Brenner DA: Liver fibrosis. J Clin Invest 2005;115:209–218.
9 Pinzani M, Rombouts K, Colagrande S: Fibrosis in chronic liver diseases: diagnosis and management. J Hepatol 2005;42:S22–S26.
10 Dienstag JL: The role of liver biopsy in chronic hepatitis C. Hepatology 2002;36: S152–S160.
11 Gebo KA, Herlong HF, Torbenson MS, et al: Role of liver biopsy in management of chronic hepatitis C: a systemic review. Hepatology 2002;36:161–172.
12 Regev A, Berho M, Jeffers LJ, Milikowski C, et al: Sampling error and intraobserver variation in liver biopsy in patients with chronic HCV infection. Am J Gastroenterol 2002;97: 2614–2618.
13 Bedossa P, Dargère D, Paradis V: Sampling variability of liver fibrosis in chronic hepatitis C. Hepatology 2003;38:1449–1457.
14 Omata M: A strategy of the treatment for the viral hepatitis (in Japanese). J Jpn Soc Int Med 2004;93:269–276.
15 Manning DS, Afdhai NH: Diagnosis and quantitation of fibrosis. Gastroenterology, 2008;134:1670–1681.
16 Wai CT, Greenson JK, Fontana RJ, et al: A simple noninvasive index can predict both significant fibrosis and cirrhosis in patients with chronic hepatitis C. Hepatology 2003; 38:518–526.
17 Imbert-Bismut F, Ratziu, Pieroni L, Charlotte F, et al: Biochemical markers of liver fibrosis in patients with hepatitis C virus infection: a prospective study. Lancet 2001;357: 1069–1075.
18 Forns X, Ampurdanes S, Llovet JM, et al: Indentification of chronic hepatitis C patients without hepatic fibrosis by a simple predictive model. Hepatology 2001;36:986–992.
19 Freeman MP, Vick CW, Taylor KJ, et al: Regenerating nodules in cirrhosis: sonographic appearance with anatomic correlation. AJR Am J Roentgenol 1986;146:533–536.
20 Ishikawa H, Ono M, Goto M, et al: Ultrasonographic findings in patients with liver cirrhosis; relationships between parenchymal, superficial echo patterns, and histological findings (in Japanese). Jpn J Med Ultrason 1990;17:522–529.
21 Fujimoto K, Yamamoto Y, Waki H, et al: Tissue characterization using integrated backscatter in viral chronic liver disease. J Ultrasound Med 1999;18(suppl):472.
22 Kumada T, Toyoda H, Ogawa S, et al: Quantification of fibrosis in hepatitis C using statistics analysis tool of ultrasonics (2nd report). Jpn J Med Ultrasonics 2007;34:S641.
23 Ziol M, Handra-Luca A, Kettaneh A, et al: Noninvasive assessment of liver fibrosis by measurement of stiffness in patients with chronic hepatitis C. Hepatology 2005;41:48–54.
24 Joo I, Choi BI: New Paradigm for management of hepatocellular carcinoma by imaging. Liver Cancer 2012;1:94–109.
25 Sandrin L, Fourquet B, Hasquenoph JM, et al: Transient elastography: a new noninvasive method for assessment of hepatic fibrosis. Ultrasound Med Biol 2003;29:1705–1713.
26 Foucher J, Chanteloup E, Vergniol J, et al: Diagnosis of cirrhosis by transient elastography (FibroScan): a prospective study. Gut 2006;55:403–408.
27 Fraquelli M, Rigamonti C, Casazza G, et al: Reproducibility of transient elastography in the evaluation of liver fibrosis in patients with chronic liver disease. Gut 2007;56:968–973.
28 Kim DY, Kim SU, Park JY, Ahn SH, Song KJ, Han KH: FibroScan based risk estimation of HBV-related HCC occurrence: development and validation of a predictive model. Liver Cancer 2012;1:123.
29 Friedrich-Rust M, Wunder K, Kriener S, et al: Liver fibrosis in viral hepatitis: noninvasive assessment with acoustic radiation force impulse imaging versus transient elastography. Radiology 2009;252:595–604.
30 Shiina T, Nitta N, Ueno E, et al: Real time tissue elasticity imaging using the combined autocorrelation method. J Med Ultrasonics 1999;26:57–66.
31 Shiina T, Nitta N, Ueno E, et al: Real time tissue elasticity imaging using the combined autocorrelation method. J Med Ultrasonics 2002;29:119–128.
32 Joo I, Choi BI: New paradigm for management of hepatocellular carcinoma by imaging. Liver Cancer 2012;1:94–109.
33 Itoh A, Ueno E, Tohno E, et al: Breast disease: clinical application of US elastography for diagnosis. Radiology 2006;239:341–350.
34 Fukunari N: More accurate and sensitive diagnosis for thyroid tumors with elastography – detection and differential diagnosis of thyroid cancers. MEDIX Suppl. 2007. http://www.hitachi-medical.co.jp/tech/medix/pdf/supple/sup_05.pdf.
35 Tsutsumi M, Miyagawa T, Matsumura T, et al: Real-time balloon inflation elastography for prostate cancer detection and initial evaluation of clinic pathologic analysis, AJR Am J Roentgenol 2010;194:W471–W476.
36 Hirooka Y, Itoh A, Kawashima H, et al: Diagnosis of pancreatic disorders using contrast-enhanced endoscopic ultrasonography and endoscopic elastography. Clin Gastroenterol Hepatol 2009;7:S63–S67.
37 Fujimoto K, Wada S, Oshita M, et al: Noninvasive evaluation of hepatic fibrosis in patients with chronic hepatitis C using elastography. MEDIX Suppl. 2007. http://www.hitachi-medical.co.jp/tech/medix/pdf/supple/sup_07.pdf.
38 Tatsumi C, Kudo M, Ueshima K, et al: Noninvasive evaluation of hepatic fibrosis using serum fibrotic markers, transient elastography (FibroScan), and real-time tissue elastography. Intervirology 2008;1:S27–S33.
39 Tatsumi C, Kudo M, Ueshima K, et al: Noninvasive evaluation of hepatic fibrosis for type C chronic hepatitis. Intervirology 2010; 53:76–81.
40 Fujimoto K, Kato M, Tonomura A, et al: Non-invasive evaluation method of the liver fibrosis using real-time tissue elastography – usefulness of judgment liver fibrosis stage by Liver Fibrosis Index (LF Index) (in Japanese). Kanzo 2010;51:539–541.
41 Haralick RM, Shanmugan K, Dinstein I: Textural features for image classification. IEEE Trans Syst Man Cybern 1973;3:610–621.
42 Mittal D, Kumara V, et al: Neural network based focal liver lesion diagnosis using ultrasound images. Comp Med Imaging Graphics 2011;35:315–323.
43 Matsumura T, Shiina T, Oosaka T, et al: Development of real-time tissue elastography (in Japanese). MEDIX 2004;41:30–35.
44 Hoon L, Kim Y, Lee J: Regenerative nodules in liver cirrhosis: findings at CT during arterial portography and CT hepatic arteriography with histopathologic correlation. Radiology 1999;210:451–458.
45 Arena U, Vizzutti F, Abraldes JG, et al: Reliability of transient elastography for the diagnosis of advanced fibrosis in chronic hepatitis C. Gut 2008;57:1288–1293.
46 Vispo E, Barreiro P, Del Valle J, et al: Overestimation of liver fibrosis staging using transient elastography in patients with chronic hepatitis C and significant liver inflammation. Antivir Ther 2009;14:187–193.
47 Rifai K, Cornberg J, Mederacke I, et al: Clinical feasibility of liver elastography by acoustic radiation force impulse imaging (ARFI). Dig Liver Dis 2011;43:491–497.

J Med Ultrasonics (2013) 40:309–323
DOI 10.1007/s10396-013-0490-z

REVIEW ARTICLE

JSUM ultrasound elastography practice guidelines: basics and terminology

Tsuyoshi Shiina

Received: 21 April 2013 / Accepted: 9 May 2013 / Published online: 19 September 2013

Abstract Ten years have passed since the first commercial equipment for elastography was released; since then clinical utility has been demonstrated. Nowadays, most manufacturers offer an elastography option. The most widely available commercial elastography methods are based on strain imaging, which uses external tissue compression and generates images of the resulting tissue strain. However, imaging methods differ slightly among manufacturers, which results in different image characteristics, for example, spatial and temporal resolution, and different recommended measurement conditions. In addition, many manufacturers have recently provided a shear wave-based method, providing stiffness images based on shear wave propagation speed. Each method of elastography is designed on the basis of assumptions of measurement conditions and tissue properties. Thus, we need to know the basic principles of elastography methods and the physics of tissue elastic properties to enable appropriate use of each piece of equipment and to obtain more precise diagnostic information from elastography. From this perspective, the basic section of this guideline aims to support practice of ultrasound elastography.

Keywords Tissue elasticity · Stiffness · Elastography · Strain · Shear wave · Acoustic radiation force

T. Shiina (✉)
Department of Human Health Sciences, Graduate School of Medicine, Kyoto University, Kyoto, Japan
e-mail: shiina.tsuyoshi.6w@kyoto-u.ac.jp

Introduction

Tissue elasticity is an important characteristic which is deeply related with pathological state; For example, in case of breast tumor, most cancerous lesions become harder than normal gland tissue [1–3]. Therefore, elastography has been developed as a modality which provides novel diagnostic information regarding tissue stiffness by replacing the conventional palpation which was used for breast examination. Moreover, recently elastography has found wider applications than breast cancer diagnosis, such as in arteriosclerosis, chronic hepatitis, myocardial diseases, and monitoring for therapy by high-intensity focused ultrasound (HIFU). Ten years have passed since the first practical equipment for elastography was released in 2003 and clinical utility was demonstrated. As a result nowadays each company provides equipment which can offer elastography. The most widely available commercial elastography methods are based on "strain imaging," using external tissue compression and generating images of the resulting tissue strain. In addition, many manufacturers have provided "shear wave imaging," which provides stiffness images based upon the shear wave propagation speed. As a result, the features of each method and equipment, i.e., their merits and limitations, must be clear for their appropriate use.

The Japan Society of Ultrasonics in Medicine (JSUM) ultrasound elastography practice guidelines are written to guide users of ultrasound elastography to comprehend the features of pieces of equipment and fully utilize them for appropriate diagnosis and therapy. Guidelines consist of plural parts; the basic part aims to definitely explain the features of each method and the terminology of the elastography technologies.

Mechanical properties of tissues [4–7]

Static properties and strain

As shown by the use of palpation as a way to diagnose diseases such as breast cancer, the stiffness of tissue reflects the pathological change of tissue. Since stiffness is resistance to deformation, application of external force is required to measure stiffness of tissue. Deformation of tissue is controlled by *elasticity* and *viscosity*. Regarding elasticity, the *stress* σ (equal to the external force per unit area) is proportional to the *strain* ε (equal to the expansion per unit length), as in Hooke's law in Eq. (1), whose coefficient is the *elastic modulus* Γ.

$$\sigma_1 = \Gamma \cdot \varepsilon. \tag{1}$$

Regarding the viscosity component, the stress σ is proportional to the speed of deformation, i.e., the strain rate $d\varepsilon/dt$, through a coefficient μ known as the *viscosity coefficient*.

$$\sigma_2 = \mu \frac{d\varepsilon}{dt}. \tag{2}$$

The mechanical characteristics of general tissue consist of a complex combination of elastic and viscous components, which are often approximated using a simplified model such as the Kelvin–Voigt model.

In cases where the speed of the applied external force is slow, such as manual compression, the effect of viscosity can be disregarded. Conversely, if high-frequency vibration is applied, the viscous component will have a major effect, the extent of which will depend on the frequency.

With regard to elasticity, three types of elastic modulus (Young's modulus, shear modulus, and bulk modulus) are defined based on the method of deformation. The *Young's modulus* E is defined by the following equation when stress is applied longitudinally to a long, thin cylindrical object and strain occurs as shown in Fig. 1a:

$$\sigma = E \cdot \varepsilon_L, \tag{3}$$

where σ is the stress and $\varepsilon_L = \Delta L/L$ is the (longitudinal) strain.

In the absence of volume change, a cylindrical object becomes thinner when stretched as shown in Fig. 1. The percentage change in the radial direction, $\varepsilon_r = \Delta r/r$, is called the transverse strain, and the ratio of longitudinal strain to transverse strain,

$$\nu = \frac{\varepsilon_r}{\varepsilon_L}, \tag{4}$$

is called *Poisson's ratio*. Poisson's ratio indicates the extent of volume change caused by deformation, and ν will be no higher than 0.5, which applies in the case of an incompressible medium.

The *shear modulus* G is defined by the following equation for the shear deformation, as shown in Fig. 1b:

$$\sigma = G \cdot \varepsilon_s, \tag{5}$$

where $\varepsilon_s = \theta$ is the shear strain.

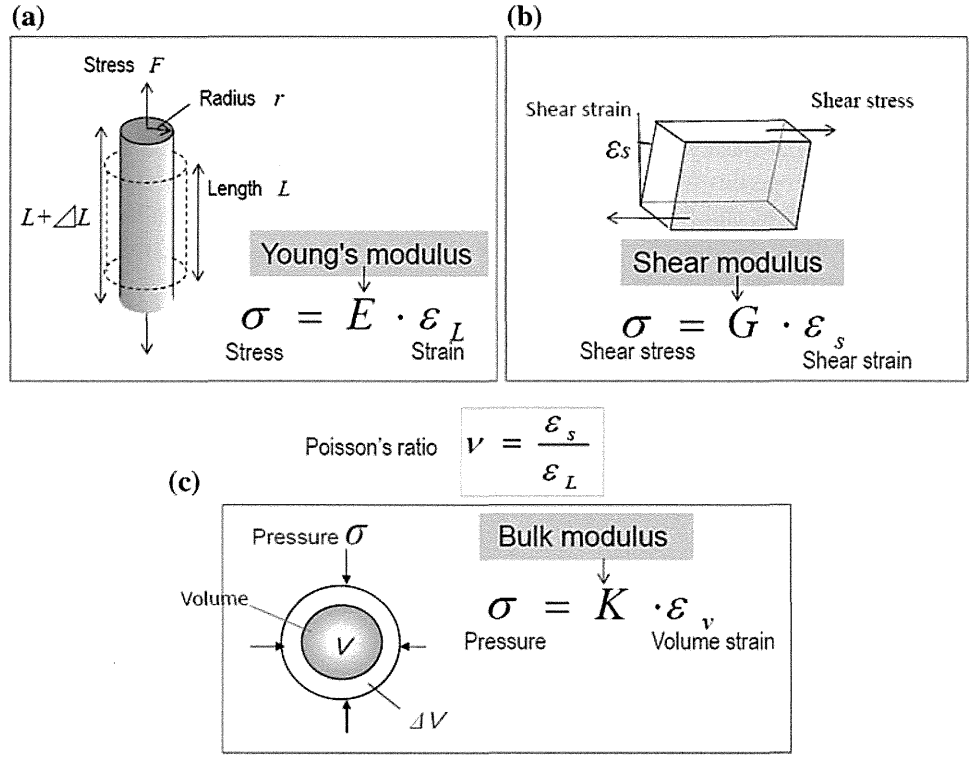

Fig. 1 Various elastic moduli

The *bulk modulus* K is defined by the following equation when the volume changes under pressure as shown in Fig. 1c:

$$\sigma = K \cdot \varepsilon_v, \tag{6}$$

where $\varepsilon_v = \Delta V/V$ is the volume strain. The larger the elastic modulus is, the smaller the strain will be for the same stress, so the material will be stiffer. These three elastic moduli are related to each other; For example, the Young's modulus E can be expressed as in Eq. (7) using the shear modulus G and Poisson's ratio v. The water content of soft tissue is high, and consequently its Poisson's ratio is near the value of 0.5 for an incompressible medium, so the Young's modulus will be equal to about three times the shear modulus, as in the following equation:

$$\begin{aligned} E &= 2(v+1)G \\ &\approx 3G. \end{aligned} \tag{7}$$

Dynamic properties and shear wave speed

The elastic modulus also determines the propagation speed of waves. Wave propagation generally involves *longitudinal waves* and *transverse waves*. The speed c_L of the longitudinal waves which are used for ordinary pulse echo images is expressed as

$$c_L = \sqrt{\frac{K}{\rho}}, \tag{8}$$

where ρ indicates the density of the medium. Using the shear modulus, the speed c_s of transverse waves is expressed as

$$c_s = \sqrt{\frac{G}{\rho}}. \tag{9}$$

In the case of soft tissue, it is known that the speed of a longitudinal wave is about the same as the speed of sound in water ($c_L = 1500$ m/s), but this means that there is little difference in K between tissues. In contrast, transverse waves, which are also called *shear waves*, attenuate rapidly and disappear in the MHz ultrasound band, but attenuation decreases and they can propagate in vivo when the frequency is below about 1 kHz. Moreover, their velocity is quite slow, i.e., $c_s = 1$–10 m/s, as compared with longitudinal waves, so G is low, i.e., 1–100 kPa, and the difference between tissues is large, enabling reconstruction of images with high tissue contrast [5].

On the other hand, unlike static deformation, *velocity dispersion* caused by the viscosity occurs during wave propagation when the frequency is high in soft tissues; For example, when the Kelvin–Voigt model is used, the following equation is used for the speed of a transverse wave instead of Eq. (9) as a result of taking into account viscosity [8]:

$$c_s = \sqrt{\frac{2\left\{G^2 + (2\pi\mu f)^2\right\}}{\rho\left\{G + \sqrt{G^2 + (2\pi\mu f)^2}\right\}}}. \tag{10}$$

Thus, c_s becomes a function of frequency f, and the higher the frequency is, the faster the speed will be.

Principle of elastography

Measured physical quantity

As mentioned in the previous section, differences in the elasticity of soft tissue are expressed by elastic moduli such as the Young's modulus E or shear modulus G.

The elastic modulus can be estimated in the following two ways according to directly measured quantities:

Strain imaging

In this method, one measures the strain ε on externally applying a stress σ, calculating E using the following equation:

$$E = \sigma/\varepsilon. \tag{11}$$

However, in practice, instead of elastic modulus, strain is used by assuming that stress is uniform, since it is difficult to know the stress within the body.

Shear wave imaging

In this method, one measures the propagation speed c_s of shear waves, calculating E or G by using Eq. (12).

$$E \approx 3G = 3\rho c_s^2. \tag{12}$$

Here, we assume that the Poisson's ratio of soft tissue is near the value of 0.5 for an incompressible medium, and that other conditions such as constant density, homogeneity, and isotropy are satisfied. Thus, the Young's modulus will be equal to about three times the shear modulus.

Excitation methods

Both of the above methods require external excitation (compression or vibration) to produce a reaction such as deformation or shear wave propagation, and a physical quantity such as strain or propagation speed is measured by using ultrasound to estimate the elasticity.

Excitation methods can be classified into (a) manual compression (using hand or cardiovascular pulsation), (b) acoustic radiation force impulse, and (c) mechanical impulse.

Classification of elastography methods

As explained in the previous section, there are two major methods based on different types of measured physical quantities and three ways to apply external excitation. Therefore, elastography is classified as presented in Table 1. Methods for integration into clinical practice are categorized into four groups as follows:

1. Stain elastography

Strain induced by quasistatic methods such as manual compression or cardiovascular pulsation is measured, and the distribution of strain or displacement within a region of interest (ROI) is displayed.

2. Acoustic radiation force impulse (ARFI) imaging

A focused acoustic radiation force "push" pulse is used to deform the tissue. The resulting tissue displacement is monitored. Although strain is the spatial differential of displacement, they are similar since both are inversely related to the tissue stiffness.

3. Shear wave elastography

Acoustic radiation force is used to generate shear waves within the organ of interest. The distribution of speed or elastic modulus converted by Eq. (12) is displayed. There is also a method which measures a local average of shear wave speed, not for imaging.

4. Transient elastography

A mechanical impulse or vibrating "punch" is used to generate shear waves. At present, commercialized technology is specialized for measuring stiffness of liver tissues and not for imaging.

The outputs obtained by each elastography technology correspond to a measured physical quantity. For strain, this includes geometric measures such as the size or shape of a low-strain area, the strain ratio of the lesion to a reference, and the E/B size ratio (the ratio of the size of a lesion in a strain image to its size in a B-mode image). For shear wave-based methods, the physical quantity is the speed itself and/or the Young's modulus converted from the shear wave speed by using Eq. (12).

Practical elastography systems

Strain elastography

The basic idea of strain elastography, i.e., measuring the tissue deformation generated by manually applying pressure with a probe on the body surface, similar to an ordinary ultrasound examination was proposed by Dr. Ophir about 20 years ago [9, 10].

Table 1 Classification of various elastography methods

Elastography methosd a)Measured physical quantity b)Output Excitation methods	**Strain imaging** a)Strain (displacement) b)Geometric measures -Strain ratio -E/B size ratio	**Shear wave imaging** a)Shear wave speed b)Shear wave speed, Young's modulus
(A)Manual compression -Palpation, -Cardiovascular pulsation	**Strain elastography** -Real-time tissue elastography™ (Hitachi Aloka) -Elastography (GE, Philips, Toshiba) -ElastoScan™ (Samsung) -eSieTouch™Elasticity Imaging (Siemens)	
(B)Acoustic radiation force impulse	**ARFI Imaging** -Virtual Touch™Imaging (Siemens)	**Shear wave elastography** -ShearWave™ Elastography: SWE (SSI) -Virtual Touch™ IQ: VTIQ (Siemens) -Virtual Touch™ Quantification: VTQ (Siemens) -ElastPQ™ (Philips))
(C)Mechanical vibration and impulse		**Transient elastography** -FibroScan™ (EchoSens)

As shown in Fig. 2, when very slight pressure (strain is about 1 %) is applied to tissue with a probe in the beam direction, the majority of the displacement will be in the direction of propagation of the ultrasound pulse, and the tissue deformation can be approximated using a one-dimensional (1D) spring model. The displacement $\delta(z)$ at each site z in the beam direction of the tissue is then calculated. This is obtained by calculating the correlation between the echo signal before and after compression. Next, the strain ε is obtained as the spatial differential of the displacement, that is, the ratio of the difference in displacement between two points to their distance pre-compression, L, as shown in Eq. (13).

$$\varepsilon = \frac{\delta_2 - \delta_1}{L}. \tag{13}$$

In fact, as described below, many technologies had to be developed to achieve real-time capability, accuracy, and stability during manual compression before it became available for clinical application [11–15].

As shown in Eq. (11), the Young's modulus E can be obtained if the stress σ and strain ε are known. However, since it is difficult to calculate the stress distribution in vivo, it is assumed to be uniform. As a result, stiff segments with large elastic modulus E will have small strain ε; therefore, strain serves as a useful indicator from the standpoint of evaluating relative stiffness.

The first practical system for ultrasound elastography was based on *strain elastography* and released in 2003 (Fig. 3). Its efficacy was demonstrated in the diagnosis of breast cancer tumors together with the elasticity score, which was proposed at the same time [16, 17] and is currently being used in various fields of clinical medicine. Nowadays, many manufacturers produce ultrasonographic equipment with a strain imaging function, as presented in Table 1.

Display methods for strain images

Strain elastography has the advantages of being easy to use and providing elasticity images with high spatial resolution in a manner similar to palpation, i.e., tissue deformation. On the other hand, strain is a relative indicator of stiffness that changes depending on the degree of compression. So, for example, the elastogram shown in Fig. 3b displays the strain normalized by the mean within the ROI in order to obtain stable images without being subject to fluctuations in the intensity of compression.

In addition, the display method of elastograms is important to relate the location in the elastogram to B-mode images. Different types of display method are used for ultrasonographic equipment, as shown in Fig. 4; For example, Dr. Ueno proposed the method applied in the first practical equipment [17]: a translucent elastogram (showing normalized strain) is superimposed in color on the corresponding B-mode image; the mean strain in the ROI is indicated in green, areas of low strain as stiff tissue in blue, and areas of high strain as soft tissue in red, as shown in Fig. 4a. Another type of display method is to display the elastogram in gray scale and the B-mode image side by side, as shown in Fig. 4b. In this case, the location in the elastogram can be indicated on the B-mode image by a cursor.

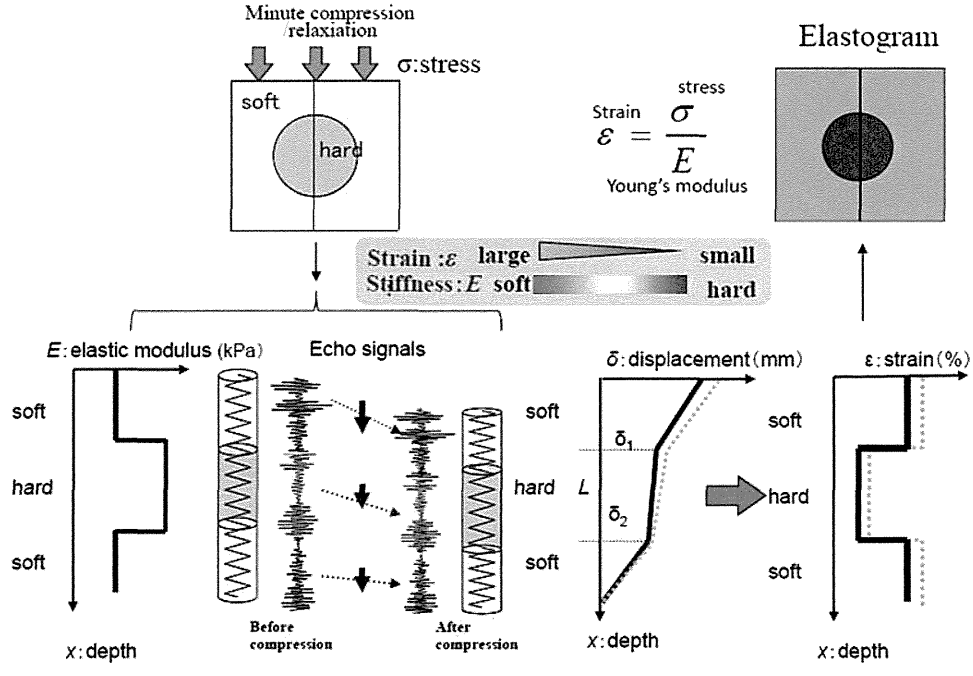

Fig. 2 Principle of strain elastography

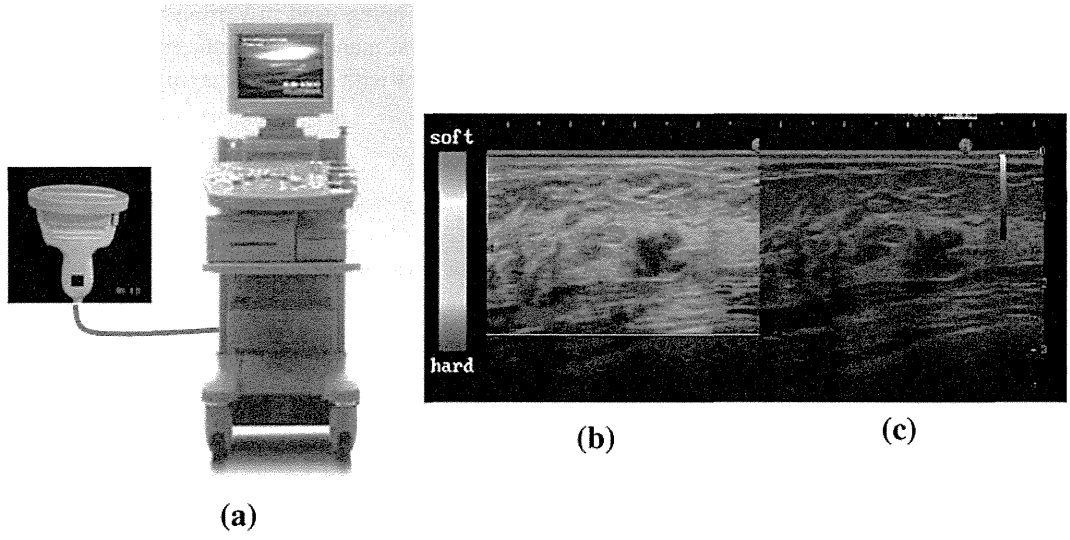

Fig. 3 Practical application of strain elastography. **a** First practical ultrasound elastography equipment, which was released for breast examination in 2003 (Real-Time Tissue Elastography, Hitachi Aloka Ltd.). **b** Elastogram (breast cancer). **c** B-mode

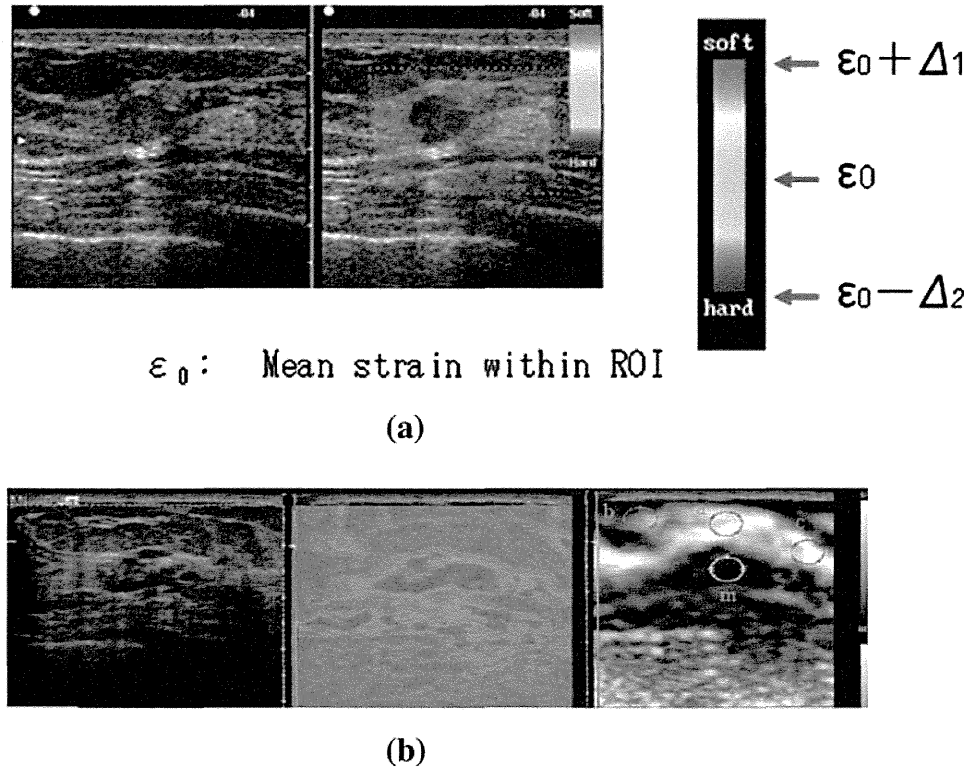

Fig. 4 Different display methods for strain images. **a** Display method applied in the first practical elastography system: the translucent elastogram within the ROI is superimposed in color on the corresponding B-mode image; the average strain in the ROI is indicated in green, areas of low strain as stiff tissue in blue, and areas of high strain as soft tissue in red (courtesy of Hitachi Aloka Medical). **b** Other display methods: elastogram superimposed on B-mode image with different color (center) and elastogram in gray scale (right) (courtesy of Siemens)

Elasticity score

Strain images depict the relative difference in elasticity between a lesion such as a mass and the surrounding tissue. Therefore, this method is suitable for detecting patterns in images. In fact, the elasticity score (Tsukuba score) is being used for breast cancer diagnosis [17]. The elasticity score is a five-point scale used to classify elastography patterns from benign to malignant as follows: score 1 (benign), score 2 (benignancy suspected), score 3 (difficult to distinguish between benign/malignant), score 4 (malignancy suspected), and score 5 (malignancy strongly suggested), as shown in Fig. 5. In the case of cysts, a specific blue–green–red pattern called the BGR sign is seen from the body surface side. This is a type of artifact, which is caused by the low level of the internal echo signals from a

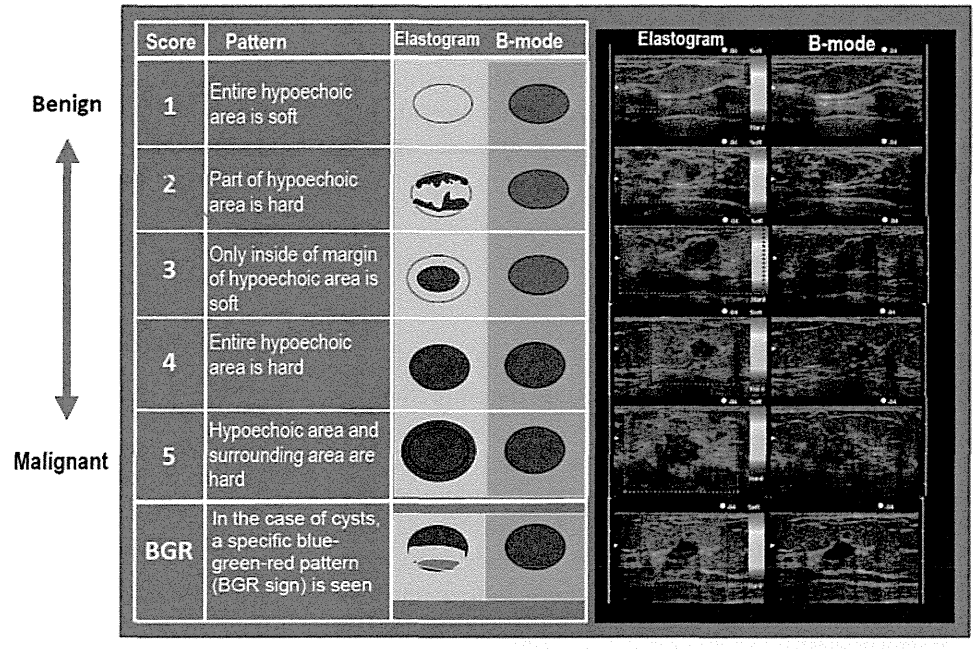

Fig. 5 Elasticity score in breast cancer diagnosis

cyst but this can be used for cyst diagnosis, like a lateral shadow on B-mode images.

Quantitative evaluation based on strain imaging

Strain imaging is basically qualitative, so it is difficult to perform quantitative comparisons between cases using strain. The fat lesion ratio (FLR) was proposed as a pseudoquantitative method. The FLR is the strain ratio between the fat and the lesion (fat in the mammary gland is used as a reference region where the change in elasticity caused by disease is minimal), as shown in Fig. 6a [18, 19].

The size of the tumor in an elastogram is often measured and compared with the size of the low-echo area in B-mode as shown in Fig. 6b, because it has been reported that malignant tumors often appear larger in strain images than in B-mode images.

Another example is a method for estimating the elastic modulus of a lesion based on the strain ratio using a coupler with known elastic modulus [20]. In addition, from elastograms of diffuse diseases such as chronic hepatitis, morphological and statistical features are extracted and analyzed for evaluation of fibrous stage, as described in the clinical section of this report.

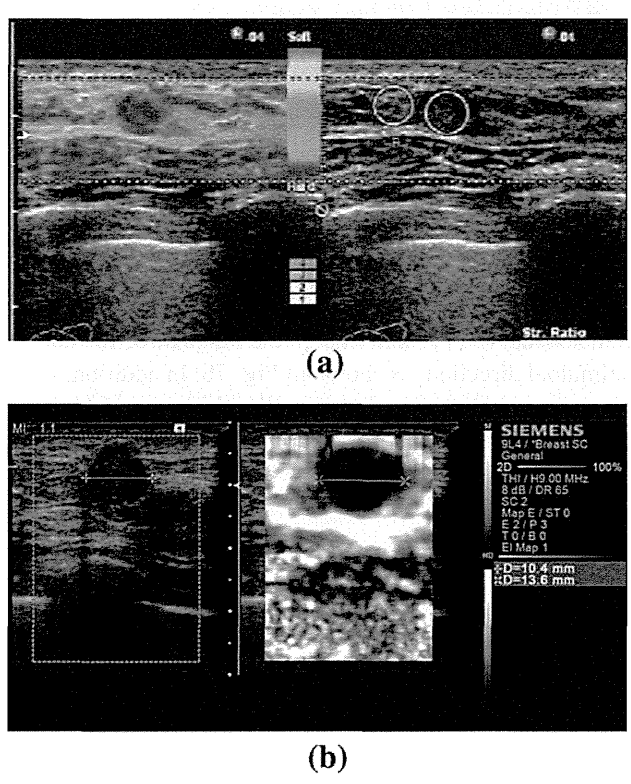

Fig. 6 Quantitative diagnosis based on strain imaging. **a** Measurement of strain ratio (courtesy of Hitachi Aloka). **b** Measurement of tumor size based on elastogram and comparison with B-mode image (courtesy of Siemens)

Displacement measurement methods

In strain imaging, displacement in the direction of pulse propagation is measured to calculate strain, while in shear wave imaging, the displacement of tissue in the direction perpendicular to the shear wave propagation is measured to calculate the speed of shear wave propagation. Therefore, measurement of displacement is a key technology in all elastography techniques, and there are several methods for measuring it. As presented in Table 1, strain elastography is now installed in ultrasound equipment from many